Potentially Singular Solutions of the 3D Axisymmetric Euler Equations

Thomas Y. Hou

Applied and Computational Mathematics
California Institute of Technology

Joint work with Guo Luo

IPAM Workshop on Mathematical Analysis of Turbulence

The Basic Problem

The 3D incompressible Euler equations are given by

$$\mathbf{u}_t + \mathbf{u} \cdot \nabla \mathbf{u} = -\nabla p, \qquad \nabla \cdot \mathbf{u} = 0,$$

with initial condition $\mathbf{u}(\mathbf{x}, 0) = \mathbf{u}_0$.

Define vorticity $\omega = \nabla \times \mathbf{u}$, then ω is governed by

$$\omega_t + (\mathbf{u} \cdot \nabla)\omega = \nabla \mathbf{u} \cdot \omega.$$

Note that $\nabla \mathbf{u}$ is related to ω by a Riesz operator K of degree zero: $\nabla \mathbf{u} = K(\omega)$, and we have $\|\omega\|_{L^p} \leq \|\nabla \mathbf{u}\|_{L^p} \leq C\|\omega\|_{L^p}$ for $1 < p < \infty$.

Thus the vortex stretching term $\nabla \mathbf{u} \cdot \omega$ is formally of the order ω^2.

Previous Work

- On the theoretical side:
  - Kato (1972): local well-posedness
  - Beale-Kato-Majda (1984): necessary and sufficient blowup criterion
  - Constantin-Fefferman-Majda (1996): geometric constraints for blowup
  - Deng-Hou-Yu (2005): Lagrangian localized geometric constraints
- Other related work:
  - Constantin-Majda-Tabak (1994): 2D surface quasi-geostrophic (SQG) equations as a model for 3D Euler
  - Cordoba (1998): no blowup of 2D SQG near a hyperbolic saddle

Previous Work (Cont'd)

- On the numerical search for singularity:
    - Grauer and Sideris (1991): first numerical study of axisymmetric flows with swirl; blowup reported away from the axis
    - Pumir and Siggia (1992): axisymmetric flows with swirl; blowup reported away from the axis
    - Kerr (1993): antiparallel vortex tubes; blowup reported
    - E and Shu (1994): 2D Boussinesq; no blowup observed
    - Boratav and Pelz (1994): viscous simulations using Kida's high-symmetry initial condition; blowup reported
    - Grauer et al. (1998): perturbed vortex tube; blowup reported
    - Hou and Li (2006): use Kerr's two anti-parallel vortex tube initial data with higher resolution; no blowup observed
    - Orlandi and Carnevale (2007): Lamb dipoles; blowup reported
- Evidence for blowup is inconclusive and problem remains open

The role of convection in 3D Euler and Navier-Stokes

In [CPAM 08], Hou and Li studied the role of convection for 3D axisymmetric flow and introduced the following new variables:

$$u_1 = u^\theta/r, \quad \omega_1 = \omega^\theta/r, \quad \psi_1 = \psi^\theta/r, \tag{1}$$

and derived the following equivalent system that governs the dynamics of u_1, ω_1 and ψ_1 as follows:

$$\begin{cases} \partial_t u_1 + u^r \partial_r u_1 + u^z \partial_z u_1 = \nu\left(\partial_r^2 + \frac{3}{r}\partial_r + \partial_z^2\right) u_1 + 2u_1 \psi_{1z}, \\ \partial_t \omega_1 + u^r \partial_r \omega_1 + u^z \partial_z \omega_1 = \nu\left(\partial_r^2 + \frac{3}{r}\partial_r + \partial_z^2\right)\omega_1 + \left(u_1^2\right)_z, \\ -\left(\partial_r^2 + \frac{3}{r}\partial_r + \partial_z^2\right)\psi_1 = \omega_1, \end{cases} \tag{2}$$

where $u^r = -r\psi_{1z}, \quad u^z = 2\psi_1 + r\psi_{1r}$.

Liu and Wang [SINUM07] showed that if **u** is a smooth velocity field, then u^θ, ω^θ and ψ^θ must satisfy: $u^\theta\big|_{r=0} = \omega^\theta\big|_{r=0} = \psi^\theta\big|_{r=0} = 0$. Thus u_1, ψ_1 and ω_1 are well defiend.

An exact 1D model for 3D Euler/Navier-Stokes

In [Hou-Li, CPAM, **61** (2008), no. 5, 661–697], we derived an excact 1D model along the z-axis for the Navier-Stokes equations:

$$(u_1)_t + 2\psi_1 (u_1)_z = \nu(u_1)_{zz} + 2 (\psi_1)_z u_1, \tag{3}$$

$$(\omega_1)_t + 2\psi_1 (\omega_1)_z = \nu(\omega_1)_{zz} + \left(u_1^2\right)_z, \tag{4}$$

$$-(\psi_1)_{zz} = \omega_1. \tag{5}$$

Let $\tilde{u} = u_1$, $\tilde{v} = -(\psi_1)_z$, and $\tilde{\psi} = \psi_1$. The above system becomes

$$(\tilde{u})_t + 2\tilde{\psi}(\tilde{u})_z = \nu(\tilde{u})_{zz} - 2\tilde{v}\tilde{u}, \tag{6}$$

$$(\tilde{v})_t + 2\tilde{\psi}(\tilde{v})_z = \nu(\tilde{v})_{zz} + (\tilde{u})^2 - (\tilde{v})^2 + c(t), \tag{7}$$

where $\tilde{v} = -(\tilde{\psi})_z$, $\tilde{v}_z = \tilde{\omega}$, and $c(t)$ is an integration constant to enforce the mean of $\tilde{v}$ equal to zero.

The 1D model is exact!

A surprising result is that the above 1D model is exact.

Theorem 1. Let u_1, ψ_1 and ω_1 be the solution of the 1D model (3)-(5) and define

$$u^\theta(r,z,t) = ru_1(z,t), \quad \omega^\theta(r,z,t) = r\omega_1(z,t), \quad \psi^\theta(r,z,t) = r\psi_1(z,t).$$

Then $(u^\theta(r,z,t),\ \omega^\theta(r,z,t),\ \psi^\theta(r,z,t))$ is an exact solution of the 3D Navier-Stokes equations.

Theorem 1 tells us that the 1D model (3)-(5) preserves some essential nonlinear structure of the 3D axisymmetric Navier-Stokes equations.

Global Well-Posedness of the full 1D Model

Theorem 2. *Assume that $\tilde{u}(z,0)$ and $\tilde{v}(z,0)$ are in $C^m[0,1]$ with $m \geq 1$ and periodic with period 1. Then the solution $(\tilde{u},\tilde{v})$ of the 1D model will be in $C^m[0,1]$ for all times and for $\nu \geq 0$.*

Proof. Differentiating the $\tilde{u}$ and $\tilde{v}$-equations w.r.t z, we get

$$
\begin{aligned}
(\tilde{u}_z)_t + 2\tilde{\psi}(\tilde{u}_z)_z - 2\tilde{v}\tilde{u}_z &= -2\tilde{v}\tilde{u}_z - 2\tilde{u}\tilde{v}_z + \nu(\tilde{u}_z)_{zz},\\
(\tilde{v}_z)_t + 2\tilde{\psi}(\tilde{v}_z)_z - 2\tilde{v}\tilde{v}_z &= 2\tilde{u}\tilde{u}_z - 2\tilde{v}\tilde{v}_z + \nu(\tilde{v}_z)_{zz}.
\end{aligned}
$$

The convection term cancels one of the nonlinear terms.

$$
(\tilde{u}_z^2)_t + 2\tilde{\psi}(\tilde{u}_z^2)_z = -4\tilde{u}\tilde{u}_z\tilde{v}_z + 2\nu\tilde{u}_z(\tilde{u}_z)_{zz}, \tag{8}
$$

$$
(\tilde{v}_z^2)_t + 2\tilde{\psi}(\tilde{v}_z^2)_z = 4\tilde{u}\tilde{u}_z\tilde{v}_z + 2\nu\tilde{v}_z(\tilde{v}_z)_{zz}. \tag{9}
$$

Another cancelltion occurs, which gives rise to

$$
\left(\tilde{u}_z^2 + \tilde{v}_z^2\right)_t + 2\tilde{\psi}\left(\tilde{u}_z^2 + \tilde{v}_z^2\right)_z = \nu\left(\tilde{u}_z^2 + \tilde{v}_z^2\right)_{zz} - 2\nu\left[(\tilde{u}_{zz})^2 + (\tilde{v}_{zz})^2\right].
$$

Construction of a family of globally smooth solutions

Theorem 3. *Let $\phi(r)$ be a smooth cut-off function and u_1, ω_1 and ψ_1 be the solution of the 1D model. Define*

$$\begin{aligned} u^\theta(r,z,t) &= r u_1(z,t)\phi(r) + \tilde{u}(r,z,t), \\ \omega^\theta(r,z,t) &= r\omega_1(z,t)\phi(r) + \tilde{\omega}(r,z,t), \\ \psi^\theta(r,z,t) &= r\psi_1(z,t)\phi(r) + \tilde{\psi}(r,z,t). \end{aligned}$$

Then there exists a family of globally smooth functioons $\tilde{u}$, $\tilde{\omega}$ and $\tilde{\psi}$ such that u^θ, ω^θ and ψ^θ are globally smooth solutions of the 3D Navier-Stokes equations with finite energy.

Potential singularity for 3D Euler equation

- Inspired by the previous study, we discover a class of initial data that lead to potentially singular solutions of 3D Euler equations.
- Main features of our study:
  - the singularity occurs at a stagnation point where the effect of convection is minimized.
  - strong symmetry (axisymmetry plus odd/even symmetry in z)
  - devises highly effective algorithms for adequate resolution
  - employs rigorous criteria for confirmation of singularity

Vorticity Kinematics

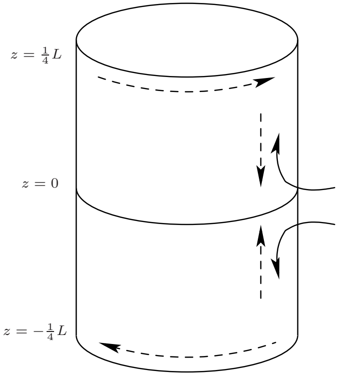

Figure : Vorticity kinematics of the 3D Euler singularity; solid: vortex lines; straight dashed lines: axial flow; curved dash lines: vortical circulation.

Local Flow Field

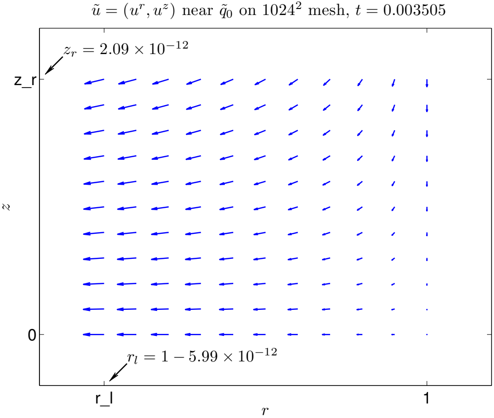

Figure : The 2D flow field $\tilde{u} = (u^r, u^z)^T$ near the maximum vorticity.

Outline

3D Axisymmetric Euler Equations

- Equations being solved: the 3D axisymmetric Euler (Hou-Li, 2008)

$$u_{1,t} + u^r u_{1,r} + u^z u_{1,z} = 2u_1\psi_{1,z},$$
$$\omega_{1,t} + u^r\omega_{1,r} + u^z\omega_{1,z} = (u_1^2)_z,$$
$$-\left[\partial_r^2 + \tfrac{3}{r}\partial_r + \partial_z^2\right]\psi_1 = \omega_1,$$

where $u_1 = u^\theta/r,\ \omega_1 = \omega^\theta/r,\ \psi_1 = \psi^\theta/r$.

  - $u^r = -r\psi_{1,z},\ u^z = 2\psi_1 + r\psi_{1,r}$: the radial/axial velocity components.

  - Initial condition:
    $u_1(r,z,0) = 100e^{-30(1-r^2)^4}\sin\left(\frac{2\pi z}{L}\right), \quad \omega_1(r,z,0) = \psi_1(r,z,0) = 0.$

  - No flow boundary condition $\psi_1 = 0$ at $r = 1$ and periodic BC in z.

Outline of the Method

- Discretization in space: a hybrid 6th-order Galerkin and 6th-order finite difference method, on an adaptive (moving) mesh that is dynamically adjusted to the evolving solution
- Discretization in time: an explicit 4th-order Runge-Kutta method, with an adaptively chosen time step

Outline

Adaptive Methods for Singularity Detection

Existing methods for computing (self-similar) singularities:

- dynamic rescaling (McLaughlin et al. 1986: nonlinear Schrödinger)
- adaptive mesh refinement (Berger and Kohn 1988: semilinear heat)
- moving mesh method (Budd et al. 1996: semilinear heat; Budd et al. 1999: nonlinear Schrödinger)

- However, these methods require knowledge of the singularity
- discrete approximation of mesh mapping functions can result in significant loss of accuracy

Our Approach: Defining the Adaptive Mesh

- We observe that vorticity tends to concentrate at a single point in the *rz*-plane.
- This motivates the development of the following special mesh adaptation strategy.
- The adaptive mesh covering the computational domain is constructed from a pair of analytic mesh mapping functions:

$$r = r(\rho), \qquad z = z(\eta),$$

where each mesh mapping function contains a small number of parameters, which are dynamically adjusted so that along each dimension a certain fraction (e.g. 50%) of the mesh points is placed in a small neighborhood of the singularity

Advancing the Solution

- The Poisson equation for ψ_1 is solved in the $\rho\eta$-space using a 6th order B-spline based Galerkin method.
- The evolutionary equations for u_1 and ω_1 are semi-discretized in the $\rho\eta$-space, where
  - the space derivatives are expressed in the $\rho\eta$-coordinates and are approximated using 6th-order centered difference scheme, e.g.

$$v_{r,ij} = \frac{v_{\rho,ij}}{r_{\rho,j}} \approx \frac{1}{r_{\rho,j}}(D^6_{\rho,0} v_i)_j$$

  - the resulting system of ODEs is integrated in time using an explicit 4th-order Runge-Kutta method

Outline

1. Introduction

2. Numerical Method
   - Overview
   - The Adaptive (Moving) Mesh Algorithm

3. Numerical Results
   - Effectiveness of the Adaptive Mesh
   - First Sign of Singularity
   - Confirming the Singularity I: Maximum Vorticity
   - Confirming the Singularity IV: Local Self-Similarity

Effectiveness of the Adaptive Mesh

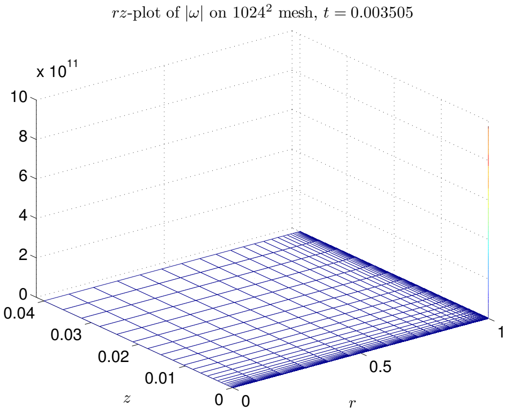

Figure : The vorticity function $|\omega|$ on the 1024×1024 mesh at $t = 0.003505$; plot shown in *rz*-coordinates with $1 : 10$ sub-sampling in each dimension.

Effectiveness of the Adaptive Mesh (Cont'd)

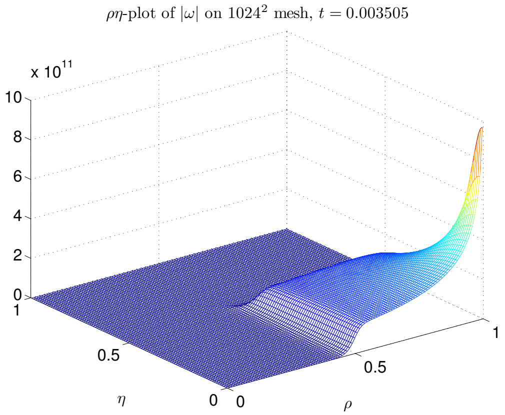

Figure : The vorticity function $|\omega|$ on the 1024×1024 mesh at $t = 0.003505$; plot shown in $\rho\eta$-coordinates with $1:10$ sub-sampling in each dimension.

Effective Mesh Resolutions

Table : Effective mesh resolutions $M_\infty,\ N_\infty$ near the maximum vorticity at selected time t.

Mesh size	$t = 0.003505$	
	M_∞	N_∞
1024×1024	1.9923×10^{12}	1.6708×10^{12}
1280×1280	2.4999×10^{12}	2.0844×10^{12}
1536×1536	2.9866×10^{12}	2.5079×10^{12}
1792×1792	3.4951×10^{12}	2.9288×10^{12}
2048×2048	3.9942×10^{12}	3.3444×10^{12}

Backward Error Analysis of the Linear Solve

Table : Backward errors of the linear solve $Ax = b$ associated with the elliptic equation for ψ_1 at $t = 0.003505$.

Mesh size	$t = 0.003505$				
	ω_1	κ_{ω_1}	ω_2	κ_{ω_2}	$\|\delta x\|_\infty / \|x\|_\infty$
512	5.9×10^{-15}	1247.3	1.9×10^{-23}	2.3×10^7	7.3×10^{-12}
768	1.1×10^{-15}	1788.84	2.1×10^{-23}	5.2×10^7	1.9×10^{-12}
1024	1.5×10^{-15}	6748.83	6.4×10^{-23}	9.3×10^7	9.9×10^{-12}

The linear system is solved using a parallel sparse direct solver called PaStiX package. Here $\omega_1, \ \omega_2$ are the componentwise backward errors of first and second kind, and $\kappa_{\omega_1}, \ \kappa_{\omega_2}$ are the componentwise condition numbers of first and second kind. It can be shown that (Arioli 1989) $\frac{\|\delta x\|_\infty}{\|x\|_\infty} \leq \omega_1 \kappa_{\omega_1} + \omega_2 \kappa_{\omega_2}$.

Outline

Maximum Vorticity

Table : Maximum vorticity $\|\omega\|_\infty = \|\nabla \times u\|_\infty$ at selected time t.

Mesh size	$\|\omega\|_\infty$		
	$t = 0$	$t = 0.0034$	$t = 0.003505$
1024×1024	3.7699×10^3	4.3127×10^6	1.2416×10^{12}
1280×1280	3.7699×10^3	4.3127×10^6	1.2407×10^{12}
1536×1536	3.7699×10^3	4.3127×10^6	1.2403×10^{12}
1792×1792	3.7699×10^3	4.3127×10^6	1.2401×10^{12}
2048×2048	3.7699×10^3	4.3127×10^6	1.2401×10^{12}

Maximum Vorticity (Cont'd)

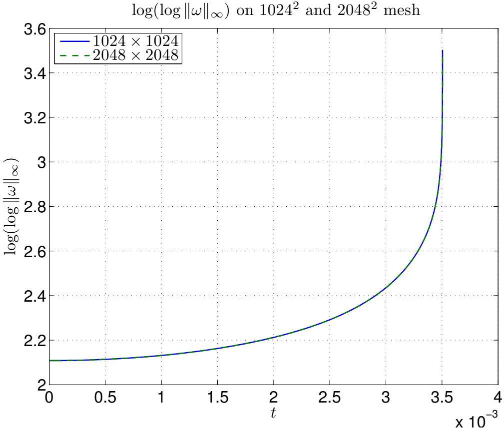

Figure : The double logarithm of the maximum vorticity, $\log(\log\|\omega\|_\infty)$, computed on the 1024×1024 and the 2048×2048 mesh.

Resolution Study on Primitive Variables

Table : Sup-norm relative error and numerical order of convergence of the transformed primitive variables u_1 at selected time t.

Mesh size	$t = 0.003505$	
	Error	Order
1024×1024	9.4615×10^{-6}	–
1280×1280	3.6556×10^{-6}	4.2618
1536×1536	1.5939×10^{-6}	4.5526
1792×1792	7.5561×10^{-7}	4.8423
Sup-norm	1.0000×10^{2}	–

Resolution Study on Primitive Variables (Cont'd)

Table : Sup-norm relative error and numerical order of convergence of the transformed primitive variables ω_1 at selected time t.

Mesh size	$t = 0.003505$	
	Error	Order
1024×1024	6.4354×10^{-4}	–
1280×1280	2.4201×10^{-4}	4.3829
1536×1536	1.1800×10^{-4}	3.9396
1792×1792	6.4388×10^{-5}	3.9297
Sup-norm	1.0877×10^{6}	–

Resolution Study on Primitive Variables (Cont'd)

Table : Sup-norm relative error and numerical order of convergence of the transformed primitive variables ψ_1 at selected time t.

Mesh size	$t = 0.003505$	
	Error	Order
1024×1024	2.8180×10^{-10}	–
1280×1280	4.7546×10^{-11}	7.9746
1536×1536	1.0873×10^{-11}	8.0925
1792×1792	2.9518×10^{-12}	8.4583
Sup-norm	2.1610×10^{-1}	–

Resolution Study on Conserved Quantities

Table : Kinetic energy E, minimum circulation Γ_1, maximum circulation Γ_2 and their maximum (relative) change over $[0, 0.003505]$.

Mesh size	$t = 0.003505$		
	$\|\delta E\|_{\infty,t}$	$\|\delta \Gamma_1\|_{\infty,t}$	$\|\delta \Gamma_2\|_{\infty,t}$
1024×1024	1.53×10^{-11}	4.35×10^{-17}	1.25×10^{-14}
1280×1280	4.17×10^{-12}	3.30×10^{-17}	7.78×10^{-15}
1536×1536	2.08×10^{-12}	3.13×10^{-17}	9.95×10^{-15}
1792×1792	6.47×10^{-13}	2.77×10^{-17}	2.14×10^{-14}
2048×2048	6.66×10^{-13}	2.53×10^{-17}	3.49×10^{-14}
Init. value	55.93	0.00	628.32

Outline

The Beale-Kato-Majda (BKM) Criterion

- The main tool for studying blowup/non-blowup: the Beale-Kato-Majda (BKM) criterion (Beale et al. 1984)

Theorem

Let u be a solution of the 3D Euler equations, and suppose there is a time t_s such that the solution cannot be continued in the class

$$u \in C([0,t];H^m) \cap C^1([0,t];H^{m-1}), \qquad m \geq 3$$

to $t = t_s$. Assume that t_s is the first such time. Then

$$\int_0^{t_s} \|\omega(\cdot,t)\|_\infty \, dt = \infty, \qquad \omega = \nabla \times u.$$

Applying the BKM Criterion

- The "standard" approach to singularity detection:
  1. assume the existence of an inverse power-law
  $$\|\omega(\cdot,t)\|_\infty \sim c(t_s - t)^{-\gamma}, \qquad c, \gamma > 0$$
  2. estimate t_s and γ using a line fitting:
  $$\left[\frac{d}{dt}\log\|\omega(\cdot,t)\|_\infty\right]^{-1} \sim \frac{1}{\gamma}(t_s - t)$$
  3. estimate c using another line fitting:
  $$\log\|\omega(\cdot,t)\|_\infty \sim -\gamma\log(\hat{t}_s - t) + \log c,$$
  where $\hat{t}_s$ is the singularity time estimated in step 2

Our Criteria

- Our criteria for choosing the fitting interval $[\tau_1, \tau_2]$:
  - τ_2 is the last time at which the solution is still "accurate"
  - choose the fitting interval $[\tau_1, \tau_2]$ in the asymptotic regime.
- Our criteria for a successful line fitting:
  - both τ_2 and the line-fitting predicted singularity time $\hat{t}_s$ converge to the same finite value as the mesh is refined; the convergence should be monotone, i.e. $\tau_2 \uparrow t_s,\ \hat{t}_s \downarrow t_s$
  - τ_1 converges to a finite value that is strictly less than t_s as the mesh is refined

Applying the Ideas: Computing the Line Fitting

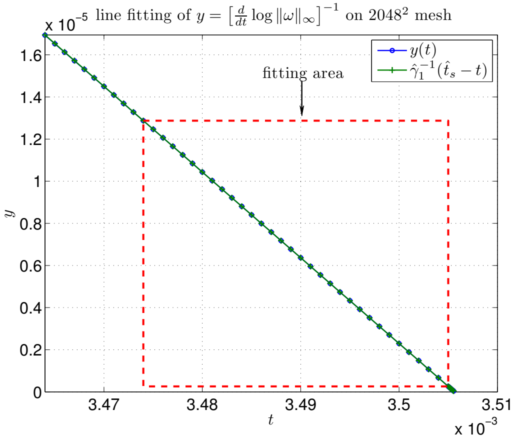

Figure : Inverse logarithmic time derivative $\left[\frac{d}{dt}\log\|\omega\|_\infty\right]^{-1}$ and its line fitting $\hat{\gamma}_1^{-1}(\hat{t}_s - t)$, computed on the 2048×2048 mesh.

Applying the Ideas: Computing the Line Fitting

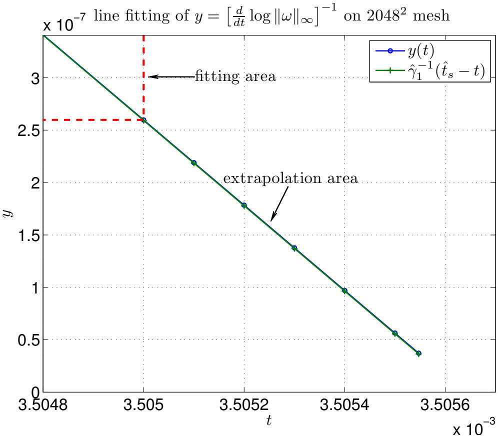

Figure : A zoom-in view of the line fitting $\hat{\gamma}_1^{-1}(\hat{t}_s - t)$.

Applying the Ideas: Computing the Line Fitting

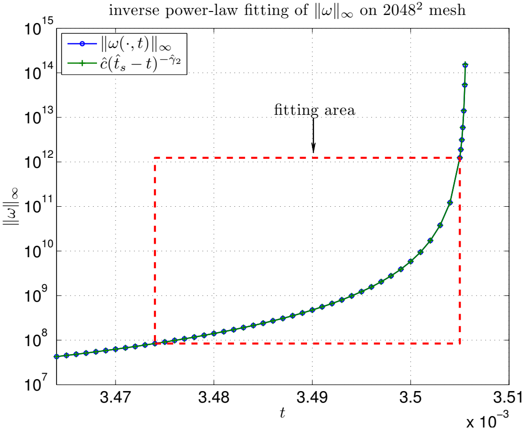

Figure : Maximum vorticity $\|\omega\|_\infty$ and its inverse power-law fitting $\hat{c}(\hat{t}_s - t)^{-\hat{\gamma}_2}$, computed on the 2048×2048 mesh.

Applying the Ideas: the “Best” Fitting Interval

Table : The “best” fitting interval $[\tau_1, \tau_2]$ and the estimated singularity time $\hat{t}_s$.

Mesh size	τ_1	τ_2	$\hat{t}_s$
1024×1024	0.003306	0.003410	0.0035070
1280×1280	0.003407	0.003453	0.0035063
1536×1536	0.003486	0.003505	0.0035056
1792×1792	0.003479	0.003505	0.0035056
2048×2048	0.003474	0.003505	0.0035056

Applying the Ideas: Results of the Line Fitting

Table : The best line fittings for $\|\omega\|_\infty$ computed on $[\tau_1, \tau_2]$.

Mesh size	$\hat{\gamma}_1^\dagger$	$\hat{\gamma}_2^\ddagger$	$\hat{c}$
1024×1024	2.5041	2.5062	4.8293×10^{-4}
1280×1280	2.4866	2.4894	5.5362×10^{-4}
1536×1536	2.4544	2.4559	7.4912×10^{-4}
1792×1792	2.4557	2.4566	7.4333×10^{-4}
2048×2048	2.4568	2.4579	7.3273×10^{-4}

†: $\hat{\gamma}_1$ is computed from $\left[\frac{d}{dt}\log\|\omega\|_\infty\right]^{-1} \sim \gamma^{-1}(t_s - t)$.

‡: $\hat{\gamma}_2$ is computed from $\log\|\omega\|_\infty \sim -\gamma\log(\hat{t}_s - t) + \log c$.

Conclusion: the maximum vorticity develops a singularity $\|\omega\|_\infty \sim c(t_s - t)^{-\gamma}$ at $t_s \approx 0.0035056$ (recall $t_e \approx 0.00350555$)

Comparison with Other Numerical Studies

Table : Comparison of our results with other numerical studies. K: Kerr (1993); BP: Boratav and Pelz (1994); GMG: Grauer et al. (1998); OC: Orlandi and Carnevale (2007); τ_2: the last time at which the solution is deemed "well resolved".

Studies	τ_2	t_s	Effec. res.	Vort. amp.
K	17	18.7	$\leq 512^3$	23
BP	$1.6^\dagger$	2.06	1024^3	180
GMG	1.32	1.355	2048^3	21
OC	2.72	2.75	1024^3	55
Ours	0.003505	0.0035056	$(3 \times 10^{12})^2$	3×10^8

†: According to Hou and Li (2008).

Nonlinear alignment of vortex stretching

- The vorticity direction $\xi = \omega/|\omega|$ could also play a role!
- Recall the vorticity equation

$$|\omega|_t + \boldsymbol{u} \cdot \nabla|\omega| = \alpha|\omega|,$$

where $\alpha = \xi \cdot \nabla \boldsymbol{u} \cdot \xi$ is the vorticity amplification factor

$$\alpha = \xi \cdot \nabla \boldsymbol{u} \cdot \xi = \xi \cdot S\xi, \qquad S = \frac{1}{2}(\nabla \boldsymbol{u} + \nabla \boldsymbol{u}^T),$$

thus the growth of α depends on the eigenstructure of S

Spectral Dynamics

- Due to symmetry, S has
  - 3 real eigenvalues $\{\lambda_i\}_{i=1}^3$ (assuming $\lambda_1 \geq \lambda_2 \geq \lambda_3$), and
  - a complete set of orthogonal eigenvectors $\{w_i\}_{i=1}^3$
- We discover, at the location of the maximum vorticity, that:
  - the vorticity direction ξ is perfectly aligned with w_2, i.e.

$$\lambda_2 = \alpha = \frac{d}{dt}\log\|\omega\|_\infty \sim c_2(t_s - t)^{-1}$$

  - the largest positive/negative eigenvalues satisfy

$$\lambda_{1,3} \sim \pm\frac{1}{2}\|\omega\|_\infty \sim \pm c(t_s - t)^{-2.457}$$

The DHY Non-blowup Criterion

- Essential ideas of DHY: no blowup if, among other things,
  - the divergence of ξ, $\nabla \cdot \xi$, and
  - the curvature $\kappa = |\xi \cdot \nabla \xi|$,

  along a vortex line do not grow "too fast" compared with the "diminishing rate" of the length of the vortex line
- Similar in spirit to CFM but more localized

Checking Against the DHY Criterion

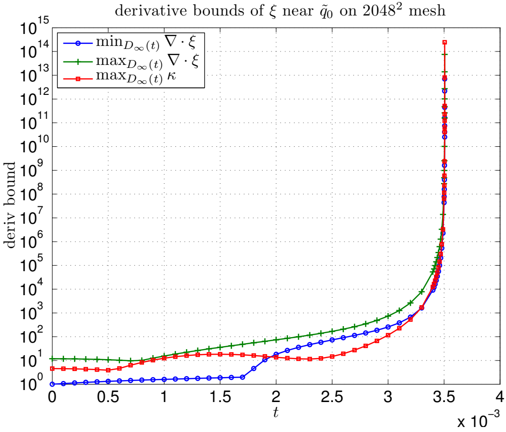

Figure : The maximum/minimum of $\nabla \cdot \xi$ and κ in a local neighborhood $D_\infty(t)$ of the maximum vorticity.

Geometry of the Vorticity Direction (Cont'd)

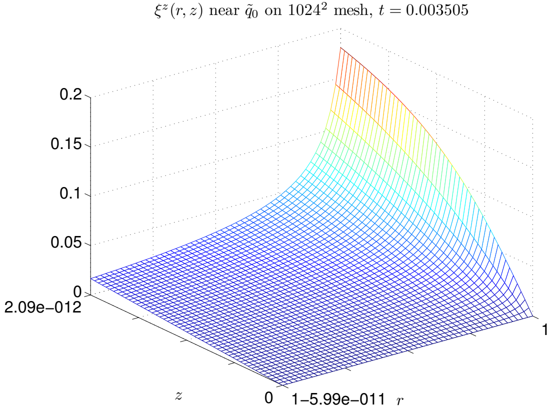

Figure : The z-component ξ^z of the vorticity direction ξ near the maximum vorticity. Note the rapid variation of ξ^z in z.

Outline

1. Introduction
2. Numerical Method
   - Overview
   - The Adaptive (Moving) Mesh Algorithm
3. Numerical Results
   - Effectiveness of the Adaptive Mesh
   - First Sign of Singularity
   - Confirming the Singularity I: Maximum Vorticity
   - Confirming the Singularity IV: Local Self-Similarity

Locally Self-Similar Solutions

- Solutions of the 3D Euler equations in $\mathbb{R}^3$ have special scaling properties:

$$u(x,t) \longrightarrow \lambda^{\alpha} u(\lambda x, \lambda^{\alpha+1} t), \qquad \lambda > 0,\ \alpha \in \mathbb{R}$$

- Can this give rise to a (locally) self-similar blowup?

$$\nabla u(x,t) \sim \frac{1}{t_s - t} \nabla U\left(\frac{x - x_0}{[t_s - t]^{\beta}}\right), \qquad x \in \mathbb{R}^3$$

- Recent results by D. Chae (2007,2010,2011) seem to give a negative answer under some strong (exponential) decay assumption on the self-similar profile ∇U.

Self-Similar Solutions with Axis-Symmetry

- In axisymmetric flows, self-similar solutions naturally take the form

$$u_1(\tilde{x},t) \sim (t_s - t)^{\gamma_u} U\left(\frac{\tilde{x}-\tilde{x}_0}{\ell(t)}\right),$$
$$\omega_1(\tilde{x},t) \sim (t_s - t)^{\gamma_\omega} \Omega\left(\frac{\tilde{x}-\tilde{x}_0}{\ell(t)}\right),$$
$$\psi_1(\tilde{x},t) \sim (t_s - t)^{\gamma_\psi} \Psi\left(\frac{\tilde{x}-\tilde{x}_0}{\ell(t)}\right), \qquad \tilde{x} \to \tilde{x}_0,\ t \to t_s^-,$$

where $\tilde{x} = (r,z)^T$ and $\ell(t) \sim [\delta^{-1}(t_s - t)]^{\gamma_\ell}$ is a length scale, and the exponents satisfy

$$\gamma_\omega = -1, \qquad \gamma_\psi = -1 + 2\gamma_\ell, \qquad \gamma_u = -1 + \frac{1}{2}\gamma_\ell.$$

This would give rise to $\|\nabla u(\cdot,t)\|_\infty \sim c(t_s - t)^{\gamma_u - \gamma_\ell}$.

Identifying a Self-Similar Solution

- We remark that the recent result of Chae-Tsai on non-existence of self-similar solutions of 3D axisymmetric Euler does not apply to our solution since they assume $|U(\xi)| \to 0$ as $|\xi| \to \infty$.
- In our case, we found that $U(0) = \Psi(0) = \Omega(0) = 0$, and $|U(\xi)| \approx c_0|\xi|^\beta$ for some $0 < \beta < 1$ as $|\xi| \to \infty$, where β satisfies $\gamma_u = \gamma_\ell \beta$ with $\gamma_u > 0$ and $\gamma_\ell > 0$. This gives $u(1, z, t_s) \approx c_0 z^\beta$ at the singularity time.
- To identify a "self-similar neighborhood", consider

$$C_\infty(t) = \left\{(r, z) \in D \colon |\omega(r, z, t)| = \tfrac{1}{2}\|\omega(\cdot, t)\|_\infty\right\}$$

Existence of Self-Similar Neighborhood

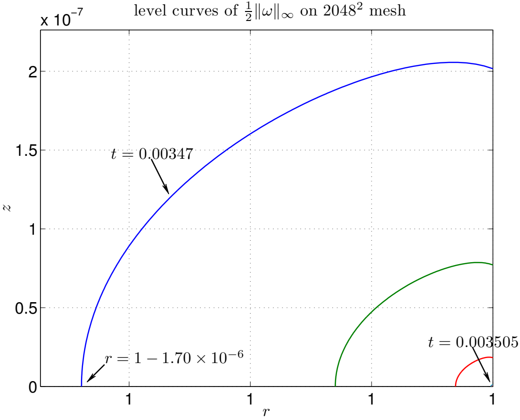

Figure : The level curves of $\frac{1}{2}\|\omega\|_\infty$ in linear-linear scale at various time instants.

Existence of Self-Similar Neighborhood (Cont'd)

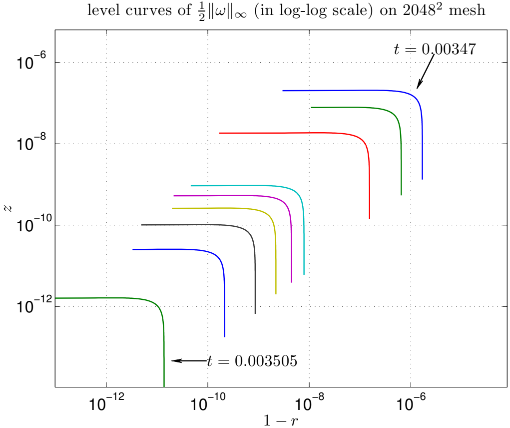

Figure : The level curves of $\frac{1}{2}\|\omega\|_\infty$ in log-log scale (against the variables $1 - r$ and z) at various time instants. Note the similar shapes of all curves.

Existence of Self-Similar Neighborhood (Cont'd)

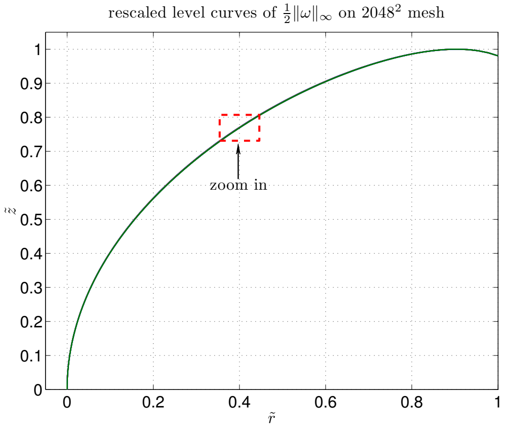

Figure : The rescaled level curves of $\frac{1}{2}\|\omega\|_\infty$.

Indication of Self-Similarity in 2D

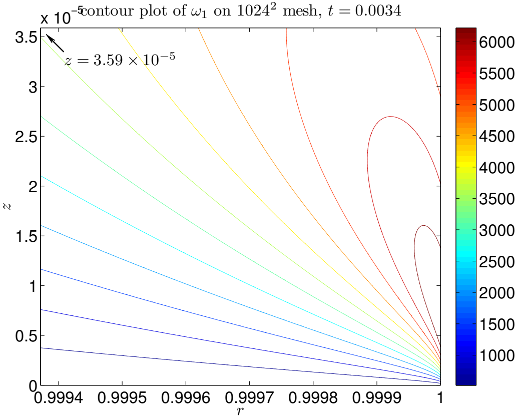

Figure : The contour plot of ω_1 near the maximum vorticity at $t = 0.0034$.

Indication of Self-Similarity in 2D (Cont'd)

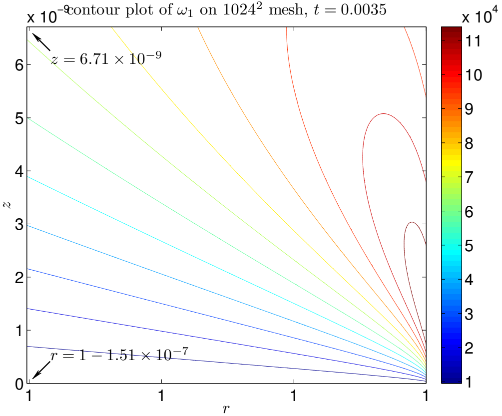

Figure : The contour plot of ω_1 near the maximum vorticity at $t = 0.0035$.

Indication of Self-Similarity in 2D (Cont'd)

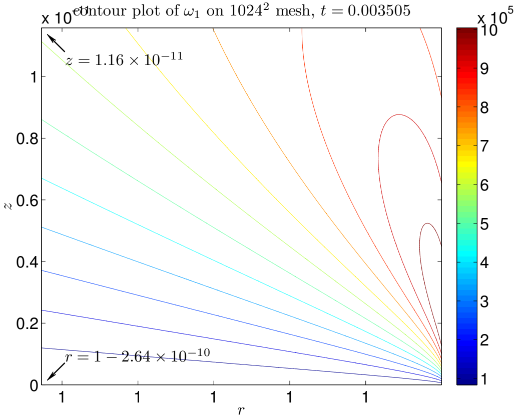

Figure : The contour plot of ω_1 near the maximum vorticity at $t = 0.003505$.

The Scaling Exponents

Table : Scaling exponents of ℓ, u_1, ω_1, and ψ_1.

Mesh size	$\hat{\gamma}_\ell$	$\hat{\gamma}_u$	$\hat{\gamma}_\omega$	$\hat{\gamma}_\psi$
1024×1024	2.7359	0.4614	-0.9478	4.7399
1280×1280	2.9059	0.4629	-0.9952	4.8683
1536×1536	2.9108	0.4600	-0.9964	4.8280
1792×1792	2.9116	0.4602	-0.9966	4.8294
2048×2048	2.9133	0.4604	-0.9972	4.8322

$\gamma_\ell \geq 1$: consistent with the *a posteriori* bound $\|u\|_\infty \leq C$

Consistency Check

Table : Consistency check for the scaling exponents.

Mesh size	$-1+\frac{1}{2}\hat{\gamma}_\ell$	$-1+2\hat{\gamma}_\ell$	$\hat{\gamma}_u-\hat{\gamma}_\ell$
1024×1024	0.3679	4.4717	-2.2745
1280×1280	0.4530	4.8118	-2.4430
1536×1536	0.4554	4.8215	-2.4508
1792×1792	0.4558	4.8232	-2.4514
2048×2048	0.4567	4.8266	-2.4529
Ref. value	$\hat{\gamma}_u$: 0.4604	$\hat{\gamma}_\psi$: 4.8322	$\hat{\gamma}_1$: 2.4568

$\|\omega\|_\infty \sim c(t_s-t)^{-2.45}$: consistent with Chae's nonexistence results

Recent progress on the blow-up of a 1D model

- One can gain important understanding of the blowup mechanism by studying a 1D model along the boundary at $r = 1$.
- We propose the following 1D model at $r = 1$ ($\rho = u_1^2$, $u = u^z$):

$$\begin{aligned} \rho_t + u\rho_z &= 0, \qquad z \in (0, L), \\ \omega_t + u\omega_z &= \rho_z \end{aligned}$$

  where the velocity u is defined by $u_z(z) = H\omega(z)$ with $u(0) = 0$.
- This 1D model and the 3D Euler equations shares many similar properties, including all the symmetry properties along z direction.
- Recently, with Drs. K. Choi, A. Kiselev, G. Luo, V. Sverak, and Y. Yao, we have proved the finite time blowup of the 1D model.

Comparison between the 1D model and the 3D Euler

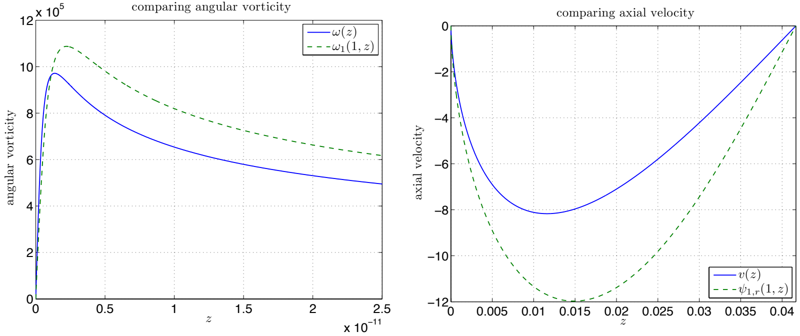

Comparison of numerical solutions of the 1D model with 3D Euler. (a) angular vorticity, and (b) axial velocity.

Blow-up of the 1D model

The main blow-up result is stated in the following theorem:
Theorem 4 (Choi, Hou, Kiselev, Luo, Sverak and Yao) For any initial data $\rho_0 \in H^2,\ \omega_0 \in H^1$ such that

(i) ρ_0 is even and ω_0 is odd at $z = 0,\ \frac{1}{2}L$,

(ii) $\rho_{0z},\ \omega_0 \geq 0$ on $[0, \frac{1}{2}L]$, and

(iii) $\int_0^{L/2} \left[\rho_0(z) - \rho_0(0)\right]^2 dz > 0$, then the solution of the 1D model develops a singularity in finite time.

One can show that the solution of the 1D model satisfies:

1. ρ is even and $\omega,\ u$ are odd at $z = 0,\ \frac{1}{2}L$ for all $t \geq 0$;
2. $\rho_z,\ \omega \geq 0$ and $u \leq 0$ on $[0, \frac{1}{2}L]$ for all $t \geq 0$.

Sketch of the proof

The analysis relies on the two lemmas, which reveal the key properties of the "Biot-Savart" law due to the strong symmetry of the flow.

Lemma 1 Let $\omega \in H^1$ be odd at $z = 0$ and let $u_z = H(\omega)$ the velocity field. Then for any $z \in [0, L/2]$,

$$u(z)\cot(\mu z) = -\frac{1}{\pi}\int_0^{L/2} K(z, z')\omega(z')\cot(\mu z')\,dz', \tag{10}$$

where $\mu = \pi/L$ and

$$K(x, y) = s\log\left|\frac{s+1}{s-1}\right| \qquad \text{with} \qquad s = s(x, y) = \frac{\tan(\mu y)}{\tan(\mu x)}. \tag{11}$$

Furthermore, the kernel $K(x, y)$ has the following properties:

1. $K(x, y) \geq 0$ for all $x,\ y \in (0, \frac{1}{2}L)$ with $x \neq y$;
2. $K(x, y) \geq 2$ and $K_x(x, y) \geq 0$ for all $0 < x < y < \frac{1}{2}L$;
3. $K(x, y) \geq 2s^2$ and $K_x(x, y) \leq 0$ for all $0 < y < x < \frac{1}{2}L$.

Sketch of the proof – continued

Lemma 2 Let the assumptions in Lemma 1 be satisfied and assume in addition that $\omega \geq 0$ on $[0, \frac{1}{2}L]$. Then for any $a \in [0, \frac{1}{2}L]$,

$$\int_a^{L/2} \omega(z) \big[u(z) \cot(\mu z) \big]_z \, dz \geq 0. \tag{12}$$

Now we are ready to prove the finite time blowup of the 1D model. Consider the integral

$$I(t) := \int_0^{L/2} \rho(z,t) \cot(\mu z) \, dz. \tag{13}$$

Sketch of the proof – continued

To prove the finite-time blowup of $I(t)$, we consider

$$\frac{d}{dt}I(t) = -\int_0^{L/2} u(x)\rho_x(x)\cot(\mu x)\,dx$$
$$= \frac{1}{\pi}\int_0^{L/2} \rho_x(x)\int_0^{L/2} \omega(y)\cot(\mu y)K(x,y)\,dy\,dx,$$

where in the second step we have used the representation formula (10) from Lemma 1.

By the assumption on the initial data, we have $\rho_x,\ \omega \geq 0$ on $[0, \frac{1}{2}L]$. Moreover, from Lemma 1, we have $K \geq 0$ for $y < x$, and $K \geq 2$ for $y > x$. Thus, we get

$$\frac{d}{dt}I(t) \geq \frac{2}{\pi}\int_0^{L/2} \rho_x(x)\int_x^{L/2} \omega(y)\cot(\mu y)\,dy\,dx.$$

Sketch of the proof – continued

It remains to find a lower bound for the right hand side, which involves some delicate dynamic estimates. With some work, we can show that

$$\begin{aligned}
\frac{d}{dt} I(t) &\geq \frac{2}{\pi} \int_0^t \int_0^{L/2} \rho_y(y,s) \cot(\mu y) \int_0^{\tilde{\xi}(t)} \rho_x(x,t)\, dx\, dy\, ds \\
&= \frac{2}{\pi} \int_0^t \int_0^{L/2} (\rho \rho_y)(y,s) \cot(\mu y)\, dy\, ds \\
&= \frac{\mu}{\pi} \int_0^t \int_0^{L/2} \rho^2(y,s) \csc^2(\mu y)\, dy\, ds \\
&\geq \frac{\mu}{\pi} \int_0^t \int_0^{L/2} \rho^2(y,s) \cot^2(\mu y)\, dy\, ds \\
&\geq \frac{2\mu}{\pi L} \int_0^t \left(\int_0^{L/2} \rho(y,s) \cot(\mu y)\, dy \right)^2 ds = \frac{2}{L^2} \int_0^t I^2 ds.
\end{aligned}$$

Self-similar Singularity of the CKY Model, joint with P. Liu

To understand the self-similar singularity of 3D axisymmetric Euler equations observed in our numerical simulation. We consider the 1D CKY model defined on $[0, 1]$,

$$\begin{cases} \partial_t \omega(x,t) + u(x,t)\partial_x \omega(x,t) = \rho_x(x,t), \\ \partial_t \rho(x,t) + u(x,t)\partial_x \rho(x,t) = 0, \\ u(x,t) = -x \int_x^1 \frac{\omega(y,t)}{y} dy. \end{cases} \tag{14}$$

This model can be viewed as a local approximation of the 3D Euler equations on the solid boundary of the cylinder with

$$\omega \sim \omega_1, \quad \rho \sim u_1^2. \tag{15}$$

The formation of finite-time singularity of this model under certain initial conditions has been proved by Choi, Kiselev and Yao.

We consider the following self-similar ansatz:

$$\begin{cases} \rho(x,t) = (T-t)^{c_\rho}\rho\left(\frac{x}{(T-t)^{c_l}}\right), \\ u(x,t) = (T-t)^{c_u}U\left(\frac{x}{(T-t)^{c_l}}\right), \\ \omega(x,t) = (T-t)^{c_w}W\left(\frac{x}{(T-t)^{c_l}}\right). \end{cases}$$

Plug these ansatz into the equations, we get

$$c_w = -1, \quad c_u = c_l - 1, \quad c_\rho = c_l - 2,$$

and a non-linear non-local ODE system

$$\begin{cases} (2-c_l)\rho(\xi) + c_l\xi\rho'(\xi) + U(\xi)\rho'(\xi) = 0, \\ W(\xi) + c_l\xi W'(\xi) + U(\xi)W'(\xi) - \rho'(\xi) = 0, \\ U(\xi) = -\xi\int_\xi^{+\infty}\frac{W(\eta)}{\eta}d\eta. \end{cases}$$

Summary of main findings of the CKY model

For this 1D model problem, we get the following results:

- We prove the existence of a family of self-similar profiles, corresponding to different leading order non-vanishing derivative of $\rho^{(s)}(\xi) \neq 0$ at $\xi = 0$.
- We analyze the far-field behavior of the profiles. They are analytic with respect to a transformed variable $\theta = \xi^{-1/c_l}$. This result can explain the Hölder continuity of the velocity field at singularity time observed in numerical simulation.

Summary of main findings of the CKY model – continued

- The asymptotic scaling exponents and self-similar profiles we construct agree with those obtained from direct numerical simulation of the CKY model.
- The self-similar profiles we construct have some stability property based on our numerical simulation. For fixed initial leading order non-vanishing derivative of $\rho^{(s)}(x,0) \neq 0$ at $x = 0$, the solutions converge to the same profile for different initial conditions of ω.

Sketch of proof:

- The Biot-Savart law for this model can be written as a local relation with a global constraint,

$$\left(\frac{U(\xi)}{\xi}\right)' = \frac{W(\xi)}{\xi}, \quad U'(0) + \int_0^\infty \frac{W(\eta)}{\eta} d\eta = 0.$$

- We first ignore the global constraint, and construct the local solutions near $\xi = 0$ using power series.
- The local solutions can be extended to the whole R^+.
- The global constraint in the Biot-Savart law determines the asymptotic scaling exponent, c_l, which depends on s only, where $\rho^{(s)}(0) \neq 0$.
- Once c_l is fixed, all other scaling exponents for u, ρ and ω can be expressed in terms of c_l.

Summary

- Main contributions of our study: discovery of potentially singular solutions of the 3D Euler equations
- Similar singularity formation also observed in 2D Boussinesq equations for stratified flows
- The singularity occurs at a stagnation point where the effect of convection is minimized.
- Strong symmetry of the solution plus the presence of the physical boundary seem to play a crucial in generating a stable and substainable locally self-similar blowup.
- Analysis of the corresponding 1D model sheds new light to the blowup mechanism.
- Analysis of the 2D Boussinesq and 3D Euler is more challenging and is under investigation.

References

- G. Luo and T. Y. Hou, *Potentially Singular Solutions of the 3D Axisymmetric Euler Equations,*, PNAS, Vol. 111, no. 36, pp. 12968-12973, 2014. Doi: 10.1073/pnas.1405238111
- G. Luo and T. Y. Hou, *Toward the Finite-Time Blowup of the 3D Incompressible Euler Equations: a Numerical Investigation*. Accepted by SIAM MMS, 2014.
- K. Choi, T. Y. Hou, A. Kiselev, G. Luo, V. Sverak, and Y. Yao *On the Finite-time Blowup of a 1D Model fro the 3D Axisymmetric Euler Equations*, arXiv:1407.4776v1 [math.AP].
- T. Y. Hou and P. Liu, *Self-Similar Singularity for a 1D Model of the 3D Axisymmetric Euler Equations*, arXiv:1407.5740v1 [math.AP].